ORIGINAL RESEARCH PAPER

Fuel Cells DOI: 10.1002/fuce.201300202

High Polymer Content 3,5-Pyridine-Polybenzimidazole Copolymer Membranes with Improved Compressive Properties

M. A. Molleo[1], X. Chen[2], H. J. Ploehn[2], K. J. Fishel[1], B. C. Benicewicz[1]*

[1] Department of Chemistry and Biochemistry, University of South Carolina, Columbia, SC 29208, USA
[2] Department of Chemical Engineering, University of South Carolina, Columbia, SC 29208, USA

Received September 12, 2013; accepted December 10, 2013; published online January 15, 2014

Abstract

Three series of polybenzimidazole (PBI) copolymers (3,5-pyridine-r-2OH-PBI, 3,5-pyridine-r-*para*-PBI, and 3,5-pyridine-r-*meta*-PBI) were polymerized and cast into membranes by the polyphosphoric acid (PPA) process. Monomer pairs with high and low solubility characteristics were used to define phase stability-processing windows for preparing membranes with high temperature membrane gel stability. Creep compliance of these membranes (measured in compression at 180 °C) generally decreased with increasing polymer content. Membrane proton conductivities decreased linearly with increasing membrane polymer content. Fuel cell performances of some high-solids 3,5-pyridine-based copolymer membranes (up to 0.66 V at 0.2 A cm^{-2} following break-in) were comparable to *para*-PBI (0.68 V at 0.2 A cm^{-2}) despite lower phosphoric acid (PA) loadings in the high solids membranes. Long-term steady-state fuel cell studies showed 3,5-pyridine-r-*para*-PBI copolymers maintained a consistent fuel cell voltage of >0.6 V at 0.2 A cm^{-2} for over 2,300 h. Phosphoric acid that was continuously collected from the long-term study demonstrated that acid loss is not a significant mode of degradation for these membranes. The PBI copolymer membranes' reduced high-temperature creep and long-term operational stability suggests that they are excellent candidates for use in extended lifetime electrochemical applications.

Keywords: Creep Compliance, Fuel Cells, Gels, Mechanical Properties, Membranes, Phase Diagrams, Polybenzimidazole, PPA Process

1 Introduction

Polymer electrolyte membrane (PEM) fuel cells, also known as proton exchange membrane fuel cells, have gained much attention over the past several decades as efficient energy conversion devices for both mobile and stationary applications [1, 2]. The type of electrolyte dopant determines the operation conditions of the fuel cell. State-of-the-art perfluorosulfonic acid (PSFA)-based PEMs, such as DuPont's Nafion, depend on water clusters to transport protons from the anode to the cathode. Since the operational temperature range is limited by the evaporation of water, these fuel cells have a low tolerance to fuel impurities and require a complicated humidification system. In contrast, PA-doped polybenzimidazole (PBI)-based PEMs have been shown to operate at temperatures up to 200 °C with higher tolerances to fuel impurities, smaller heat exchangers, and no humidification requirements [3–8].

The conventional process for preparing PBI membranes involves PBI film casting from an organic solvent, solvent evaporation, and subsequent imbibing of PA by the membrane [9–13]. In contrast, the PPA Process offers a more facile route to processing PBI membranes [3, 4, 14–16]. Diacid monomers are polymerized with tetraamines in PPA under nitrogen at typical temperatures of 190–220 °C. This simple one-pot reaction produces PBIs of high molecular weight that are completely dissolved in PPA. The polymerization solution can be directly cast to produce films of uniform thickness. The cast polymer films are then placed into a PA bath or a controlled humidity chamber to hydrolyze the PPA into PA. Since PA is a poor solvent for many PBIs, the film undergoes a sol-to-gel transition which produces a gel membrane

[*] *Corresponding author, benice@sc.edu*

fully imbibed with PA. This produces a Type 3 Flory gel, one with polymer networks formed by physical aggregation of polymer chains [17]. Excess water and PA generated through the hydrolysis process are drained from the membranes prior to characterization and use.

Both the PA content and the membrane morphology are influenced by the membrane processing technique. Membranes processed conventionally from organic solvents and subsequently imbibed with PA tend to contain less PA than those cast from the PPA Process. Additionally, a comparative study of the two casting techniques showed that two *meta*-PBI membranes with similar PA content had different proton conductivities [18]. The PPA Process generated a membrane with a higher conductivity, 0.13 S cm^{-1}, compared with 0.048 S cm^{-1} from a conventionally cast membrane. Because these two membranes had the same chemical composition (polymer type, molecular weight, and PA content), this demonstrated that the casting technique plays a fundamental role in the determination of the membrane properties.

Studies over the last decade have shown that PBI membranes have outstanding fuel cell performance [16, 19, 20]. Fuel cells employing poly(2,2′-(1,4-phenylene)5,5′-bibenzimidazole) (*para*-PBI) cast from the PPA Process has been shown to operate for over 15,000 h under steady-state conditions (>0.6 V at 0.2 A cm^{-2}) [5]. However, little is known about the membrane's resistance to long-term degradation modes including polymer creep and membrane thinning, which can result in gas crossover, voltage degradation, and the eventual quenching of the fuel cell. For stationary fuel cell applications, the Department of Energy has an operational target of 40,000 h for 2014 [21]. To reach this goal, enhancement of the mechanical properties of PBI membranes is of great importance to prevent membrane creep and enhance the fuel cell lifetimes. One study investigated the mechanical properties of a low polymer content PBI-based MEA at 180 °C [22] and confirmed that the contact stress in the MEA decreased with time. Initial creep and compression properties of commercially available Nafion membranes at elevated temperatures (70–90 °C) have been documented; however, these water-based membranes have inherent mechanical issues at elevated temperatures due to dehydration of the polymer matrix [23–25]. Studies on the high temperature creep properties in compression have not been reported for PBI membranes, despite the importance of such properties for long-term fuel cell operation.

New approaches to improving the long-term mechanical properties of PBI membranes are needed which are cost effective and compatible with the manufacturing processes that have been developed for these unique membrane materials. One way to improve the mechanical properties of PBI membranes may be to increase the polymer content of the gel membrane. However, the processability of the PBI/PPA solution into a film is limited by the solubility of the polymer and viscosity of the solution. If the polymer content increases beyond a critical point, the solution becomes unprocessable because (1) not all of the polymer can be dissolved in the PPA solution, and/or (2) the solution becomes too viscous to cast into a membrane. *para*-PBI, for example, can only be cast with a polymer content up to approximately 5 wt.%. This limitation can be circumvented by synthesizing functionalized PBI polymers made from more soluble monomers. Increasing polymer solubility enables film casting from more concentrated solutions, leading to membranes with higher polymer content.

A wide variety of soluble PBIs, prepared via the PPA Process, have been investigated as candidates for high temperature fuel cell membranes [19]. Functionalized polybenzimidazoles, such as dihydroxy-PBI (2OH-PBI), were shown to improve proton transport and thermal stability of the gel membrane [4]. Figure 1 compares the relative solubility and gel stability of four common functionalized PBIs. Dihydroxy-PBI has a unique network of phosphate branches and crosslinks that both lowers the solubility of the polymer in PPA and increases its chemical stability (inferred from its poor solubility in concentrated sulfuric acid). Pyridine-based polybenzimidazoles (py-PBI) have been investigated because of their higher solubility in polyphosphoric acid (PPA), which was attributed to their higher concentration of basic sites (imidazole and imine groups) [26]. Additionally, PBI monomers that have *meta*-oriented constituents are generally more soluble than *para*-oriented PBIs due to their improved backbone flexibility. This increased solubility of the PBIs only has minor effects on the thermal stability of the PBI itself, retaining degradation temperatures above 350 °C. However, increasing the solubility of the PBIs has been shown to decrease the gel stability of the film at elevated temperatures. Our previous research has shown that 3,5-pyridine-PBI is too soluble in PA to form a stable gel membrane at room temperature [26].

Our prior work thus shows a fundamental limitation of PBI homopolymers for preparing gel membranes (Figure 1). Increasing monomer solubility leads to higher membrane polymer content, but it has a negative impact on membrane thermal stability. In this work, we report the synthesis of novel PBI copolymers for membranes with high polymer content as well as high gel thermal stability. Specifically, we prepared three sets of copolymers by the PPA Process: 3,5-pyridine-r-

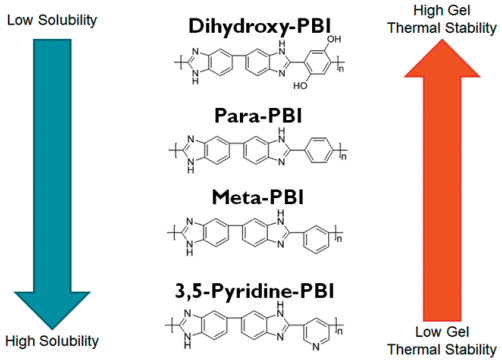

Fig. 1 Comparison of PBI polymer chemistries – and their relative, qualitative impact on gel thermal stability and polymer solubility in PPA and PA.

ORIGINAL RESEARCH PAPER

2OH-PBI, 3,5-pyridine-r-*para*-PBI, and 3,5-pyridine-r-*meta*-PBI copolymers. The highly soluble 3,5-pyridine moiety was used to impart higher polymer solubility in PPA, and therefore, higher polymer content in the membranes. Thus, copolymerizations of 3,5-pyridinedicarboxylic acid and TAB with dihydroxyterephthalic acid, terephthalic acid, and isophthalic acid were conducted to explore the relative solubilities and gel membrane stabilities. Membranes with higher polymer solids than previous work were prepared and characterized with regard to fuel cell performance as well as creep under compressive stress at high temperature. The current study reports the relationships between PBI chemical structure and membrane composition with the fundamental properties of gel stability, membrane conductivity, mechanical properties, and fuel cell performance.

2 Experimental

2.1 Chemicals

3,5-Pyridinedicarboxylic acid was purchased from Acros Chemical, TCI America, and Yongyi Chemicals Group Co., Ltd (~98% purity) and purified by recrystallization from a 1:10 dilution of concentrated hydrochloric acid prior to use. 2,5-Dihydroxyterephthalic acid was purchased from Fisher Scientific and Sigma–Aldrich, and it was purified by recrystallization from a 3:2 dilution of absolute ethanol to deionized water prior to use. Terephthalic acid (TPA, purified) and isophthalic acid (IPA, purified) were purchased from Amoco Chemicals and used as received. 3,3′,4,4′-Tetraaminobiphenyl (TAB, purified) and polyphosphoric acid (PPA, 115%) were donated by BASF Fuel Cells and used as-received.

2.2 Polybenzimidazole Synthesis and Membrane Preparation

To a three-necked flask equipped with nitrogen flow and overhead stirrer, a solution of 3,5-pyridinedicarboxylic acid (py-2COOH), 3,3′,4,4′-tetraaminobiphenyl (TAB), polyphosphoric acid (PPA), and either isophthalic acid (IPA), terephthalic acid (TPA), or 2,5-dihydroxyterephthalic acid (2OH-TPA) was stirred and heated to 195–220 °C for 3–30 h. This polymerization scheme is detailed in Scheme 1. The polymerization time correlated with both monomer concentration and ratio of the pyridine monomer to the other diacid monomer. Both the stir-rate and the temperature were adjusted during the polymerization. At the end of the polymerization, the PBI solution was poured onto a pyrex or glass plate and cast at a thickness of 15 mil using a Gardner blade. To form a gel membrane, the glass plates with the cast films were immediately placed into a humidity controlled chamber at 55 ± 5% relative humidity (RH), 25 ± 2 °C. Complete hydrolysis of the membranes occurred over 12–24 h. The final gel membrane thickness was approximately 300–500 µm.

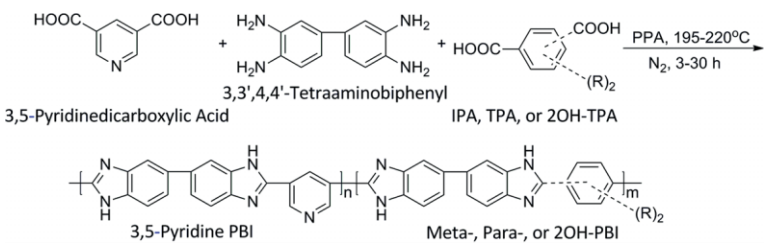

Scheme 1 Synthesis of random copolymers using 3,5-pyridinedicarboxylic acid and TAB with terephthalic acid (R = H), isophthalic acid (R = H), or 2,5-dihydroxyterephthalic acid (R = –OH).

2.3 Characterization Techniques

The composition of acid-doped PBI membranes was determined by measuring the relative amounts of polymer solids, water, and acid in the film. The PA content was determined by titrating a sample of membrane with standardized sodium hydroxide solution (0.1 N) using a Metrohm 716 DMS Titrino autotitrator. The sample was washed with water and dried in an oven overnight at 120 °C. The dried sample was then weighed to determine polymer solids content for the membrane. The amount of water was calculated by subtracting the weights of polymer and PA from the initial PBI membrane sample weight.

Thermal analysis and inherent viscosity measurements were performed on polymer isolated from the PPA Process. Following the polymerization of the random copolymers, the polymer/PPA solution was hydrolyzed in deionized water and the polymer was mechanically blended into small particles. The polymer was filtered and placed in an oven overnight at 120 °C to dry the sample. Thermogravimetric analysis (TGA) was performed using a TA Instruments TGA Q-5000 IR with a heating rate of 10 °C min^{-1} under nitrogen. Differential scanning calorimetry (DSC) was conducted using a TA Instruments DSC Q-2000 with a nitrogen flow rate of 20 mL min^{-1} and heating and cooling rates of 10 °C min^{-1}. Inherent viscosities (IV's) were measured in concentrated sulfuric acid at 30.0 °C and 0.2 g dL^{-1} concentration using an Ubbelohde viscometer. The following equation was used to calculate the IV:

$$\ln[(t)(t_0)^{-1}]c^{-1} = IV(\mathrm{dL\ g^{-1}}) \quad (1)$$

The tensile properties of the membranes were tested at room temperature using an Instron Model 5543A system with a 10 N load cell and crosshead speed of 5 mm min^{-1}. Dog-bone shaped specimens were cut according to ASTM standard D683 (Type V specimens) and preloaded to 0.1 N prior to testing.

The compression creep tests were performed using a TA Instruments RSAIII dynamic mechanical analyzer (DMA). Discs were cut from polymer membranes with a diameter of 6.3 mm and thickness of approximately 0.9–1.2 mm. Sample conditioning was found to be essential for obtaining reproducible measurements. Before the compression creep tests, the samples were conditioned by placing them between two parallel smooth Teflon

blocks at 180 °C for approximately 24 h. Little or no compressive stress was applied, but the blocks kept the sample discs flat while the water and PA content equilibrated. The sample was then transferred directly into the DMA. In a typical compression creep test, a step stress was applied to the sample and held constant for 20 h. The deformation of the test specimen was recorded as a function of time. To ensure the compression stress was uniaxial, the compression tool surfaces were coated with PTFE to minimize the friction between the sample and the tool. The creep compliance was calculated by dividing the strain with the applied stress, and the compliance as a function of time was fitted with the Maxwell model [27]:

$$J(t) = J_s^0 + t\eta_0^{-1} \quad (2)$$

where J_s^0 represents the steady-state (recoverable) compliance, t is time, and η_0 is the extensional viscosity at zero extension rate. All tests were carried out at 180 °C, and the applied stress level was selected to be 0.1 MPa.

Frequency sweep tests were also performed using the TA Instruments RSAIII at various temperatures to characterize the thermal stability of the gel membranes. Cylindrical compression samples of 15 mm diameter and ~4 mm thickness were used. Before the tests, the samples were conditioned *in vacuo* at 80 °C for 24 h. The storage modulus (E') and loss modulus (E'') were recorded as functions of frequency at various temperatures. The test frequency spanned from 0.00249 to 9.9 Hz, and a strain amplitude of 0.25% was used.

Ionic conductivities were measured via a four-probe through-plane bulk measurement using an AC Zahner IM6e impedance spectrometer that scanned a frequency range from 1 to 100 kHz. A rectangular sample of membrane (3.5 cm × 7.0 cm) was placed in a glass cell with four platinum wire current collectors. Two outer electrodes set 6.0 cm apart supplied current to the cell, while the two inner electrodes 2.0 cm apart on opposite sides of the membrane measured the voltage drop. To ensure a through-plane bulk measurement of the membrane ionic conductivity, the two outer electrodes were placed on opposite sides of the membrane and the two inner electrodes were arranged in the same manner. The reported conductivities were of preconditioned (dried) membranes that were held at >100 °C for at least two hours. Proton conductivity was calculated using the following equation:

$$\sigma = D(LBR)^{-1} \quad (3)$$

where D was the distance between the two test current electrodes, L was the thickness of the membrane, B was the width of the membrane, and R was the measured resistance.

Membrane electrode assemblies consisted of the polymer membrane sandwiched between two electrodes. MEAs were prepared by hot pressing the acid-doped membrane between an anode electrode and a cathode electrode at 150 °C for 90–150 s using 2.0×10^4 N (4,500 lbs) of force and compressing to 80% its original thickness. Prior to compression, the membrane was pretreated with concentrated PA (<10 s) to wet its surface, thereby reducing the interfacial resistance of the membrane-catalyst interface. Electrodes were received from BASF Fuel Cell, Inc. with 1.0 mg cm^{-2} platinum (Pt) catalyst loading. Anode electrodes contained only Pt as the catalyst, while the cathode electrodes contained a BASF Fuel Cell standard cathode Pt alloy. The active area of the electrodes was 45.15 cm^2. Fuel cell fabrication was conducted by assembling the cell components as follows: end plate:anode current collector:anode flow field:MEA:cathode flow field:cathode current collector:end plate. Gaskets were used on either side of the MEA to control compression. Following assembly, the cell was evenly clamped to 5.65 N m (50 in. lbs) of pressure.

Fuel cell performance was measured on 50 cm^2 (active area 45.15 cm^2) single stack fuel cells using test stations obtained from Plug Power or purchased from Fuel Cell Technologies. Polarization curves were obtained at various temperatures (120–180 °C) with hydrogen as a fuel and different oxidants (air or oxygen gas). Fuel cells were operated for at least 100 h (break-in period) at 0.2 A cm^{-2} at 180 °C before measurement of polarization curves. Long-term stability testing was performed under static current and temperature conditions of 0.2 A cm^{-2} and 180 °C with constant flow rates of hydrogen and air. Degradation rates of long-term fuel cell operations were calculated by linear fitting of cell voltage data points with respect to time. Product water and PA from the exhaust gases were collected by passing the gases through bottles containing distilled water. The PA loss was determined by analyzing the water in the collection bottles using an ascorbic acid test and UV–Vis absorbance at 880 nm wavelength [28].

3 Results and Discussion

3.1 Synthesis and Characterization of Random Copolymers

Three series of 3,5-pyridine-r-2OH-PBI, 3,5-pyridine-r-*para*-PBI, and 3,5-pyridine-r-*meta*-PBI copolymers were polymerized and cast into membranes using the PPA Process. The ratio of pyridine monomer to either isophthalic, terephthalic, or 2,5-dihydroxyterephthalic acid was adjusted for each polymerization. Stoichiometric control of diacid:tetraamine was maintained at 1:1 for all polymerizations. The random nature of the polymerizations, particularly for the 3,5-pyridine dicarboxylic acid and dihydroxyterephthalic acid, was studied. Elemental analysis for the 50/50 copolymer polymerization for nitrogen and oxygen content did not show any deviations over a broad range of monomer conversion, thus implying the random nature of the copolymers.

Thermal analysis and inherent viscosity (IV) measurements of the copolymers were conducted on polymer samples isolated from the PPA solution as described in the Section 2.3. Differential scanning calorimetry did not show any transitions up to 350 °C and thermal gravimetric analysis showed that decomposition occurred at >400 °C in nitrogen for all of the copolymers tested. IV measurements of the copolymers yielded ranges of 1.18–1.87 dL g^{-1} for the 3,5-pyri-

dine-r-*para*-PBIs, 0.30–1.43 dL g^{-1}, for the 3,5-pyridine-r-*meta*-PBIs, and 0.60–1.02 dL g^{-1} for the 3,5-pyridine-r-2OH-PBIs. These IVs indicate low-to-moderate molecular weights for the copolymers. It was apparent that as the initial monomer concentration in the polymerizations increased, the polymerization time to attain a high solution viscosity and the resulting inherent viscosity of the polymer decreased. This trend is shown in Figure 2. Additionally, the polymerization time to reach a high viscosity that could still be cast decreased as the ratio of pyridine monomer to either terephthalic, isophthalic, or 2,5-dihydroxyterephthalic acid decreased.

3.2 Gel Film Formation

As described previously, the PPA Process is a facile route for producing PBI membranes [3]. All copolymers were cast directly from the polymerization solutions at 195–220 °C onto glass plates. Higher polymer content membranes needed to be cast thinner than the lower polymer content, traditional PPA processed membranes to produce similar thicknesses of the membranes following hydrolysis of the PPA to PA. All of the high polymer content membranes were cast at 15 mil (0.381 mm) and produced membranes with thicknesses between 0.3 and 0.5 mm. Following hydrolysis of the PPA to PA and the simultaneous sol-to-gel transition, excess water and PA were drained from the membranes prior to their characterization.

The ability to process high solids-content 3,5-pyridine-r-2OH-PBIs, 3,5-pyridine-r-*para*-PBIs, and 3,5-pyridine-r-*meta*-PBIs into gel films was dependent on both the initial monomer charge in the polymerization vessel and the ratio of the two diacid monomers. The amount of time needed to reach an appropriate viscosity suitable for film casting (judged visually) was strongly influenced by the ratio of pyridine monomer to the less soluble monomer. This trend is shown in Figure 3. Because the introduction of 2OH-, *para*-, or *meta*-PBI decreased the solubility of the copolymer in PPA, the polymerization solutions with a higher ratio of dihydroxyterephthalic acid, terephthalic acid, or isophthalic acid attained a high viscosity relatively quickly (causing a decrease in the polymerization time) and eventually reaching a viscosity where the solution no longer flows and could not be cast into a membrane. It is also important to note that the IV of the copolymers decreased concomitantly with decreasing polymerization time. As shown previously [3], high IVs are required for membranes to possess suitable mechanical properties. Thus, the low solubility of the copolymer composition, high viscosity of the polymerization solution, and decreased IV all combined to limit the copolymer compositions that could provide suitable membranes.

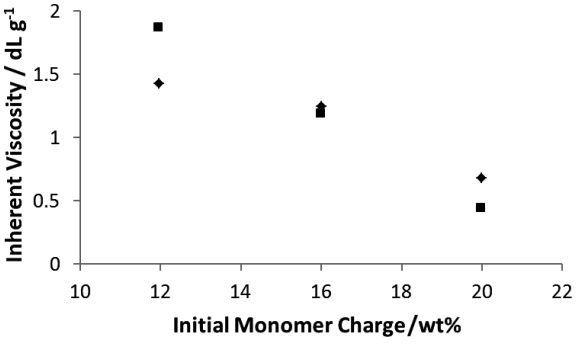

Fig. 2 The inherent viscosities of (a) 5:1 ratio (diamonds) and (b) 3:1 ratio (squares) 3,5-pyridine-r-*para*-PBIs.

3.3 Membrane Properties

To investigate the suitability of 3,5-pyridine-r-2OH-PBI, 3,5-pyridine-r-*para*-PBI, and 3,5-pyridine-r-*meta*-PBI membranes for fuel cell use, both mechanical properties and proton conductivities were measured.

Both physical touch and tensile tests indicated that the room temperature mechanical properties of all copolymers increased with increasing polymer solids content in the membrane. This trend was true for all copolymer series and shown in Figure 4 for the 3,5-pyridine-r-*para*-PBI series. All of the Young's Moduli of the random copolymers were much higher than that of *para*-PBI (<1.5 MPa at 25 °C) which had a 4.5% polymer solids content in the as-cast membrane [3].

Upon heating the copolymer films to operating conditions (180 °C), it was observed that membranes with a high ratio of 3,5-pyridine-PBI to *para*-PBI or 2OH-PBI were thermally unstable (discussed later). Similarly, almost all of the 3,5-pyridine-r-*meta*-PBI membranes exhibited thermal instability of the gel structure upon heating. Visual inspection confirmed

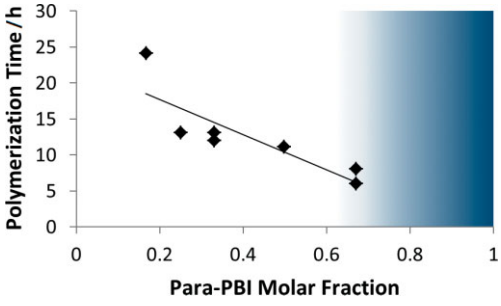

Fig. 3 Polymerization time to reach a high solution viscosity for 3,5-pyridine-r-*para*-PBIs. The blue region indicates either that the polymerization solution was too viscous to cast or that the inherent viscosity of the polymer was too low to make a stable membrane. Final polymerization temperatures were up to 220 °C with an initial monomer charge of 12 wt.%.

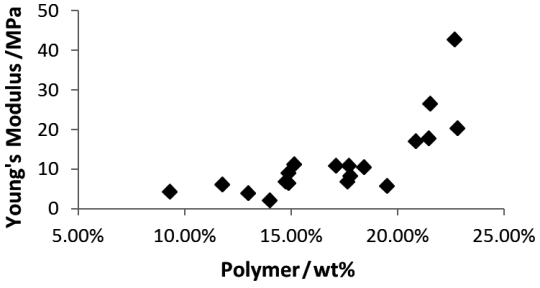

Fig. 4 Young's modulus (in tension) of 3,5-Pyridine-r-*para*-PBI as-cast membrane films measured at 25 °C.

that these gel membrane transitioned from a solid-like gel to a viscous liquid when they were heated. For this reason, 3,5-pyridine-r-*meta*-PBIs were not processed into MEAs for further high temperature electrochemical studies. Furthermore, it was determined that only specific ratios of 3,5-pyridinedicarboxylic acid to TPA or 2OH-TPA were feasible to polymerize and cast into stable membranes. If the *para*-PBI molar fraction is near unity, the polymerization solutions cannot be cast as membranes due to the low polymer IV or very high solution viscosity. Two different phenomena were responsible for the observed behavior. At low *para*-PBI copolymer content, the more soluble 3,5-pyridine monomer allowed polymerization to proceed to higher polymer IV and thus the ability to cast the polymerization solutions into membranes. However, in this composition range, the more soluble 3,5-pyridine content copolymer membranes were not stable at high temperatures. Conversely, at high *para*-PBI copolymer content, the less soluble terephthalic acid prevented the polymerization from reaching high IV. Thus, the combination of low solubility and shorter polymerization times (lower molecular weights) resulted in solutions that did not produce membranes or poor ones at best. Figure 5 illustrates the phase stability-processing maps for preparing usable membranes at initial monomer charges of 12 and 16 wt.% for 3,5-pyridine-r-*para*-PBI copolymers. Since 2OH-PBI has lower solubility than *para*-PBI, the processing window for 3,5-pyridine-r-2OH-PBI was comparatively smaller. The fuel cell performances of the membranes at the mid-composition range at 180 °C following break-in are also shown in Figure 5. The

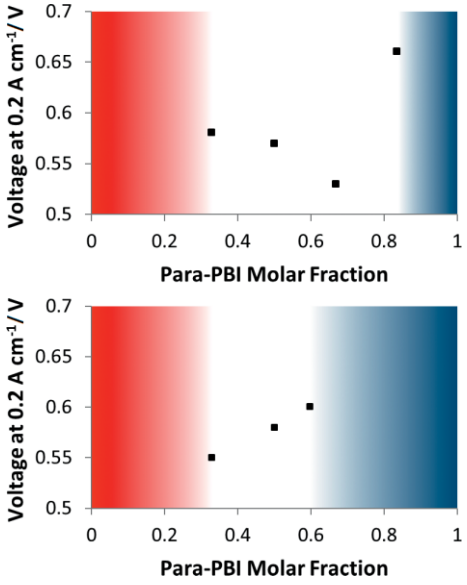

Fig. 5 Phase stability-processing maps and non-optimized fuel cell performances at 0.2 A cm^{-2} using H_2:Air at a 1.2:2.0 stoichiometric ratio (following break-in) of 3,5-pyridine-r-*para*-PBI gel films. Membranes were cast from 12 wt.% monomer charge (top) and 16 wt.% monomer charge (bottom) solutions. The red areas represent membrane compositions with poor gel thermal stability at 180 °C, and blue areas represent compositions yielding polymerization solutions that did not lead to usable cast films.

results indicate that membranes produced within these processing windows are viable for fuel cells.

To further investigate the creep resistance of the gel membranes under static compression, creep tests were performed on several high solid content membranes as well as on a commercial *para*-PBI gel membrane (low solid, ~5 wt.%) at 180 °C. The membranes were tested under anhydrous conditions to simulate fuel cell operating conditions. Figure 6 shows the creep compliance curves for a *para*-PBI, a 3,5-pyridine-r-*para*-PBI (py:*para* = 1:1), and a 3,5-pyridine-r-2OH-PBI (py:2OH = 1:1). Each compliance curve represents an average of at least two experimental data sets obtained under the same conditions. In general, the compressive creep compliance of each gel material increased with time as the result of membrane thinning under static compression. After an initial nonlinear transition period (2–4 h), the compliance appears to increase linearly with time, but the actual compliance slope (rate of increase) decreased gradually over time due to the compression of the membrane structure and the concomitant composition change. The compression creep tests yield two important metrics, creep compliance and creep rate, that can be used to evaluate a gel membrane's resistance to creep deformation. A material with good creep resistance should have low values of both creep compliance and creep rate. Comparison of the low polymer content *para*-PBI gel (<5 wt.%) with the high polymer content pyridine-PBI gels (>10 wt.%) shows that the low-solid *para*-PBI gel's compliance was more than twice those of the high-solid PBI gels after 20 h of static compression at 180 °C. In addition, the average creep rates (change of compliance over a period of time) during the last 12 h of test for the 3,5-pyridine-r-*para*-PBI and the 3,5-pyridine-r-2OH-PBI were 0.038 and 0.028 $(MPa\ h)^{-1}$, respectively, two to three times smaller than the value of 0.097 $(MPa\ h)^{-1}$ for the low-solid *para*-PBI. Hence the high-solid PBI gel membranes exhibited superior creep resistance performance relative to the low-solid PBI gel.

An accurate method of detecting the gel-to-solution transition for thermally unstable membranes was desired to streamline the selection process for high temperature electrochemical

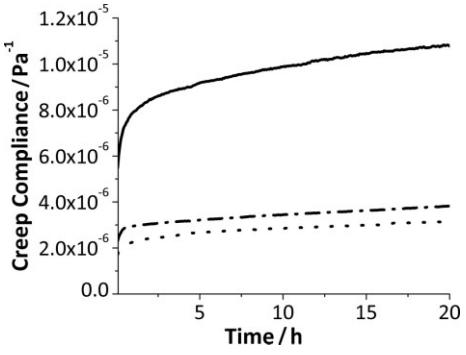

Fig. 6 Creep compliance curves of 3,5-pyridine/*para*-PBI (py:*para* = 1:1, 19.5 wt.% polymer, dotted line), 3,5-pyridine/2OH-PBI (py:2OH = 1:1, 14.6 wt.% polymer, dash-dot line) and *para*-PBI (<5 wt.% polymer, solid line) membranes, preconditioned at 180 °C for 24 h and compressed at 0.1 MPa at 180 °C.

ORIGINAL RESEARCH PAPER

characterization. A frequency sweep test at various temperatures was performed on a high polymer content membrane with known thermal instability below 180 °C. Figure 7 shows the frequency-dependent storage (E') and loss (E'') modulus curves of a 3,5-pyridine-r-*para*-PBI (py:*para* = 5:1) gel membrane. At each temperature, as ω decreased, both E' and E'' decreased. At temperatures below 140 °C, the storage modulus curve was always above the loss modulus curve in the entire measured frequency range. At temperatures above 150 °C, a crossover of E' and E'' occurred, i.e., $\tan\delta = (E'')(E')^{-1} \geq 1$, as frequency decreased. Such a crossover of E' and E'' indicates a transition from elastic, solid-like behavior to viscous, liquid-like behavior. Figure 7b shows that the transition occurred between 140 and 150 °C. The thermal instability of this membrane is attributed to the high percentage of the 3,5-pyridine moiety, as gel-to-solution transitions of similar high polymer content membranes with low 3,5-pyridine proportions are not observed. These measurements support the observation of gel thermal instabilities of select copolymer compositions.

It is well known that proton conductivity is an important property of a fuel cell membrane. In high temperature PBI fuel cell membranes, proton conductivities have previously been shown as dependent on water content, PA content, membrane morphology, and membrane chemistry [7, 12, 16, 19, 20]. Because PBI fuel cells are operated at temperatures between 160 and 180 °C, the effects of water on proton transport are considered to be minimal. Therefore, proton conductivities were measured on anhydrous membranes at temperatures ranging from 25 to 180 °C. Figure 8 shows proton conductivity and PA content of 3,5-pyridine-r-*para*-PBI membranes as functions of polymer content (wt.%). The correlation of the data sets shows that proton conductivities generally increase with increasing PA content for these PBI membranes. By adjusting the initial monomer wt.% in the polymerization, both the PA content of the final membrane and the proton conductivity could be controlled reasonably well. As long as the membrane was thermally stable up to 180 °C, there seemed to be no direct correlation between the chemistry of the high solids membranes and their respective conductivities within a copolymer series.

Figure 9 compares the dependence of the proton conductivities of Nafion, a PPA-processed *para*-PBI homopolymer membrane, and a high solids content 3,5-pyridine-r-*para*-PBI copolymer. Nafion, a perfluorosulfonic acid-based PEM that relies on water to assist proton conduction, exhibits a conductivity of approximately 0.08 S cm^{-1} at 80 °C [3, 29]. However, its ability to transport protons is drastically reduced at tem-

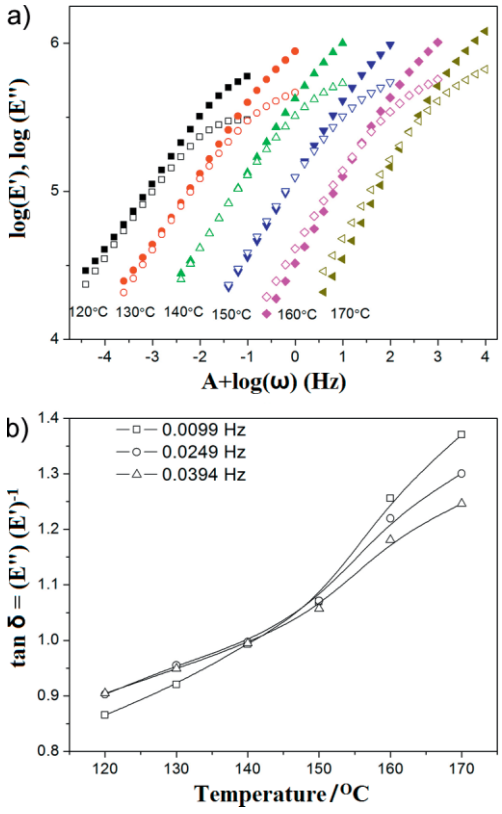

Fig. 7 (a) Storage modulus E' (filled symbols) and loss modulus E'' (open symbols) of a high polymer content 3,5-pyridine-r-*para*-PBI (py:*para* = 5:1) gel membrane as functions of oscillation frequency ω (Hz) at various temperatures. Each set of data is shifted by an integer number A (from −2 to +3) on the log frequency scale to avoid data overlap. (b) Loss tangent (tan δ) as a function of temperature at various oscillation frequencies.

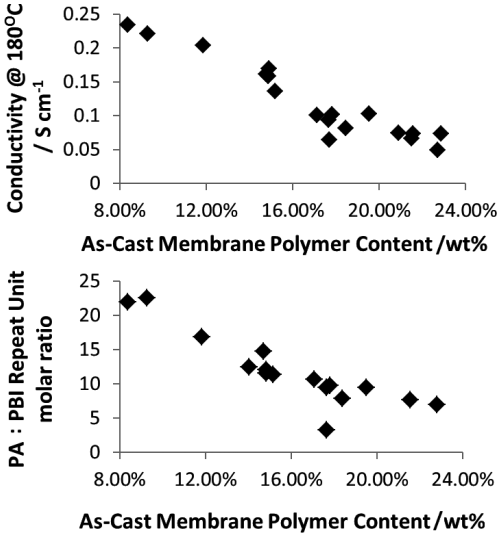

Fig. 8 Anhydrous proton conductivity of 3,5-pyridine-r-*para*-PBI membranes at 180 °C (top) and their measured PA content (bottom).

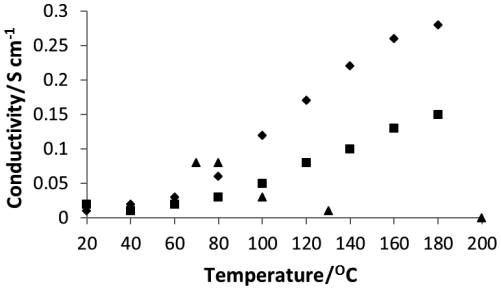

Fig. 9 Proton conductivities of membranes composed of Nafion (triangles) [29], *para*-PBI (diamonds), and 3,5-pyridine-r-*para*-PBI (py:*para* = 1:5) (squares).

peratures above 80 °C due to the evaporation of water, thus requiring a complicated humidity system for fuel cell operation. In comparison, PPA-processed PBI membranes demonstrated much higher anhydrous proton conductivities as the temperature was increased above 100 °C. This improvement of conductivities is attributed to the low vapor pressure of PA and the faster kinetics of the proton transport [30–32]. The *para*-PBI membrane exhibited higher proton conductivity than 3,5-pyridine-r-*para*-PBI membrane due to the former's higher PA content. The *para*-PBI membrane (<10 wt.% polymer) shows a proton conductivity of 0.28 S cm^{-1} with a 40:1 molar ratio of PA to polymer repeat unit (PRU); the copolymer membrane (>15 wt.% polymer) reached a proton conductivity of 0.16 S cm^{-1} with a 11.9:1 PA:PRU molar ratio. Although the copolymer membrane compositions described in this study have slightly lower anhydrous proton conductivities than *para*-PBI homopolymer membranes, the copolymer membranes show much better creep resistance (Figure 6).

It was of interest to further explore the relationship of polymer solids content in the membrane with other important fuel cell properties such as mechanical properties and conductivities. For a single copolymer ratio of 3,5-pyridine-r-*para*-PBI (py:*para* = 2:1), three membranes were prepared with varying polymer contents by polymerizing at three different monomer concentrations. Figure 10 shows the room temperature stress–strain curves for the three as-cast membranes (characterization data in Table 1). The data demonstrate that, even for a single copolymer composition that is sufficiently soluble to be polymerized at high monomer concentration, both polymer content and PA/PBI ratio can be adjusted accordingly to produce membranes with controllable compositions. Most importantly, it was shown that membranes could be produced with much higher moduli than previously reported for the PPA Process while maintaining high proton conductivities.

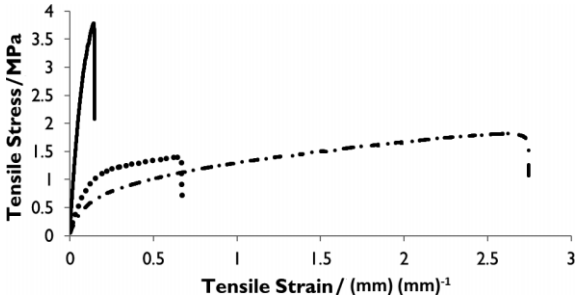

Fig. 10 Stress–strain curves of three 3,5-py-r-*para*-PBI as-cast membranes measured at 25 °C (py:*para* = 2:1). Solid line = MM1-38-5; dotted line = MM1-37-4; dot-dashed line = MM1-36-3.

Steady-state fuel cell tests were performed on many 3,5-pyridine-r-*para*-PBI and 3,5-pyridine-r-2OH-PBI membranes at 180 °C. All MEAs constructed from high polymer content membranes were surface pretreated (~10 s) with concentrated PA prior to MEA fabrication. This pretreatment wet the surfaces of the membrane and decreased the resistances at the anode and cathode interfaces. Long-term studies were conducted on specific copolymer membranes and the exhaust gases were passed through water bottles to trap PA for subsequent analysis.

Figure 11 shows the voltage degradation characteristics and the measured PA loss data for a 3,5-pyridine-r-*para*-PBI membrane (py:*para* = 1:5) operated at 180 °C. A very low voltage degradation rate of 5.23 μV h^{-1} was measured at 0.2 A cm^{-2} following a 100 h break-in period, which is significantly lower than *para*-PBI (60 μV h^{-1}) at 190 °C [5]. The total PA loss rate (~16.53 ng cm^{-2} h^{-1}) was an order of magnitude less than *para*-PBI (~110.4 ng cm^{-2} h^{-1}) at 190 °C [5]. These differences could partially be attributed to the difference in operating temperatures. PA loss from the cathode was greater than the PA loss from the anode which was likely affected by the water generated at the cathode. This PA loss rate, when compared to the total amount of PA in the copolymer membrane, suggests that PA loss will not be a major factor of fuel cell failure.

The long-term cell test in Figure 11 failed at 2,350 h due to a malfunction of the silicon rubber heaters of the cell hardware and subsequent overheating (>200 °C). Failure of the

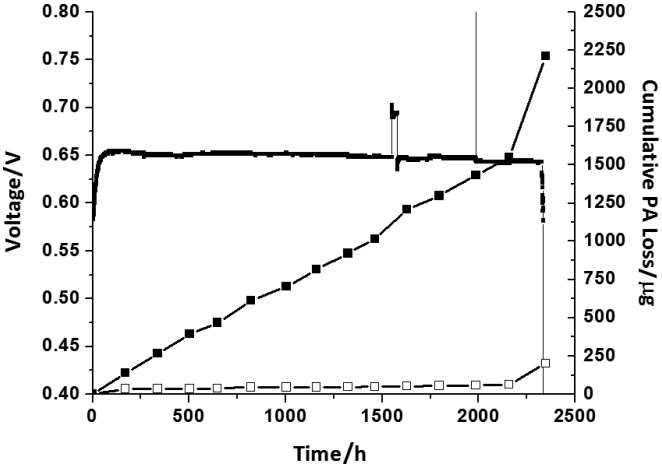

Fig. 11 Long-term steady-state performance of a 3,5-pyridine-r-*para*-PBI copolymer membrane at 180 °C. The active area of the cell was 45.15 cm^2, the current density was 0.2 A cm^{-2}, and the hydrogen:air ratio was 1.2:2.0 stoichiometric ratio. Anode PA loss (hollow squares) = 0.63 ng cm^{-2} h^{-1}, Cathode PA loss (solid squares) = 15.90 ng cm^{-2} h^{-1}, degradation rate = 5.23 μV h^{-1}.

Table 1 Comparison of polymer content in as-cast membranes with PA content, Young's modulus, and anhydrous proton conductivity of three 3,5-py-r-*para*-PBIs, where py:*para* = 2:1.

Membrane name	Polymer content (wt.%)	PA:PBI repeat unit (molar ratio)	Young's modulus (MPa)	Proton conductivity at 180 °C (S cm^{-1})
MM1-36-3	14.76	14.78	6.71	0.16
MM1-37-4	18.44	7.89	10.45	0.08
MM1-38-5	22.71	6.98	42.54	0.05

membrane was observed by the decrease in both fuel cell performance and increase in the PA loss rate.

4 Conclusion

Three series of 3,5-pyridine-r-2OH-PBI, 3,5-pyridine-r-*para*-PBI, and 3,5-pyridine-r-*meta*-PBI copolymers were polymerized and cast into membranes using the PPA Process. The ratio of 3,5-pyridine dicarboxylic acid monomer to isophthalic, terephthalic, or 2,5-dihydroxyterephthalic acid was easily adjusted for each polymerization, thereby allowing a large range of polymers to be produced. Both the initial monomer charge and the ratio of the diacid monomers were used to construct phase stability-processing maps that described copolymer compositions that could be prepared at high solids content solutions and cast into membranes.

Membranes prepared using the 3,5-pyridine-r-*meta*-PBI copolymers exhibited thermally unstable gel structures due to the high solubility of the copolymers in PA at 180 °C, or they displayed liquid-like behavior (high creep compliance) at high temperatures. Membranes prepared from 3,5-pyridine-r-*para*-PBIs and 3,5-pyridine-r-2OH-PBIs were stable at high temperatures when the amount of the more soluble 3,5-pyridinedicarboxylic acid was not too high. Copolymer compositions were identified with sufficient solubility and high temperature membrane stability to evaluate the effects of initial monomer polymerization charge on membrane composition, mechanical properties, and proton conductivity.

Long-term fuel cell tests were performed on a 3,5-pyridine-r-*para*-PBI membrane, and compared to previous results for lower solids content *para*-PBI membranes. An extremely low voltage degradation rate of 5.23 $\mu V\ h^{-1}$ was measured following a 100 h break-in period, which was significantly lower than previous results for *para*-PBI membrane (60 $\mu V\ h^{-1}$). PA loss measurements indicated that total acid loss rate (16.53 ng $cm^{-2}\ h^{-1}$) is not likely to act as a primary failure mode in steady-state operation.

Acknowledgements

The authors would like to gratefully acknowledge BASF Fuel Cell, Inc., Dr. Gordon Calundann, and Dr. Joerg Belack for technical and financial support of the work. The authors also acknowledge DARPA for partial support of this research.

References

[1] B. C. H. Steele, A. Heinzel, *Nature* **2001**, *414*, 345.
[2] D. Dunwoody, J. Leddy, *Electrochem. Soc. Interface* **2005**, *3*, 37.
[3] L. Xiao, H. Zhang, E. Scanlon, L. S. Ramanthan, E. W. Choe, D. Rogers, T. Apple , B. C. Benicewicz, *Chem. Mater.* **2005**, *17*, 5328.
[4] S. Yu, B. C. Benicewicz, *Macromolecules* **2009**, *42*, 8640.
[5] S. Yu, L. Xiao, B. C. Benicewicz, *Fuel Cells* **2008**, *8*, 1654.
[6] Q. Li, R. He, J. Gao, O. J. Jensen, N. J. Bjerrum, *J. Electrochem. Soc.* **2003**, *150*, A1599.
[7] R. He, Q. Li, G. Y. Xiao, N. J. Bjerrum, *J. Membr. Sci.* **2003**, *226*, 169.
[8] A. Chandan, M. Hattenberger, A. El-Kharouf, S. Du, A. Dhir, V. Self, B. Pollet, A. Ingram, W. Bujalski, *J. Power Sources* **2013**, *231*, 264.
[9] J. S. Wainright, J. T. Wang, D. Weng, R. F. Savinell, M. Litt, *J. Electrochem. Soc.* **1995**, *142*, L121.
[10] M. Litt, R. Ameri, Y. Wang, R. F. Savinell, J. S. Wainright, *Mater. Res. Soc. Symp. Proc.* **1999**, 313.
[11] Y. Zhai, H. Zhang, G. Liu, J. Hu, B. Yi, *J. Electrochem. Acta* **2006**, *52*, 394.
[12] Q. Li, H. A. Hjuler, N. J. Bjerrum, *J. Appl. Electrochem.* **2001**, *31*, 773.
[13] O. E. Kongstein, T. Berning, B. Borresen, F. Seland, R. Tunold, *Energy* **2006**, *32*, 418.
[14] G. Qian, B. C. Benicewicz, *J. Polym. Sci., Part A* **2009**, *47*, 4064.
[15] S. Yu, H. Zhang, L. Xiao, E. W. Choe, B. C. Benicewicz, *Fuel Cells* **2009**, *9*, 318.
[16] J. Mader, X. Lixiang, T. Schmidt, B. C. Benicewicz, *Adv. Polym. Sci.* **2008**, *216*, 63.
[17] P. J. Flory, *Faraday Discuss. Chem. Soc.* **1974**, *57*, 7.
[18] D. C. Seel, B. C. Benicewicz, L. Xiao, T. J. Schmidt, *Handb. Fuel Cells* **2009**, *5*, 300.
[19] M. Molleo, T. J. Schmidt, B. C. Benicewicz, *Encyclopedia of Sustainability, Science and Technology*, Springer Science+Business Media LLC, (Ed. R.B. Meyers), New York, USA, **2012**, p. 391.
[20] J. S. Wainright, R. F. Savinell, M. H. Litt, *Handb. Fuel Cells*, **2003**, *3*, 436.
[21] U.S. Dept. Energy, An integrated strategic plan for the research, development, and demonstration of hydrogen and fuel cell technologies, **2011**. Available at http://www1.eere.energy.gov/hydrogenandfuelcells/pdfs/program_plan2011.pdf.
[22] A. Suvorov, J. Elter, R. Staudt, R. Hamm, G. Tudryn, L. Schadler, G. Eisman, *Int. J. Solids Struct.* **2008**, *45*, 5987.
[23] K. A. Patankar, D. A. Dillard, S. W. Case, M. W. Ellis, Y.-H. Lai, C. S. Gittleman, *Fuel Cells* **2012**, *12*, 787.
[24] Y.-H. Lai, C. K. Mittelsteadt, C. S. Gittleman, D. A. Dillard, *J. Fuel Cell Sci. Technol.* **2009**, *6*, 0210021.
[25] Y. Li, D. A. Dillard, S. W. Case, M. W. Ellis, Y.-H. Lai, C. S. Gittleman, D. P. Miller, *J. Power Sources* **2009**, *194*, 873.

[26] L. Xiao, H. Zhang, T. Jana, E. Scanlon, R. Chen, E. W. Choe, L. S. Ramanthan, S. Yu, B. C. Benicewicz, *Fuel Cells* **2005**, *5*, 287.
[27] J. D. Ferry, Viscoelastic Properties of Polymers, 3rd Ed., John Wiley & Sons, New York, USA, **1980**.
[28] Standard methods for the examination of water and wastewater **1999**, Available at http://www.scribd.com/doc/44520215/Standard-Methods-for-the-Examination-of-Water-and-Waste-Water-20th-1999.
[29] R. F. Savinell, J. S. Wainright, M. H. Litt, *Proc. Electrochem. Soc*. **1998**, *98–27*, 81.
[30] L. Vilciauskas, S. J. Paddison, K.-D. Kreuer, *J. Phys. Chem. A* **2009**, *113*, 9193.
[31] T. Dippel, K. D. Kreuer, J. C. Lassegues, D. Rodriguez, *Solid State Ionics* **1993**, *61*, 41.
[32] A. Bozkurt, M. Ise, K. D. Kreuer, W. H. Meyer, G. Wegner, *Solid State Ionics* **1999**, *125*, 225.

